In Vitro Bioactivity Test of Real Dental Implants According to ISO 23317

Martina Kolafová[1]/Jan Šťovíček[2]/Jakub Strnad, PhD[3]/Josef Zemek, PhD[4]/Jiři Dybal, PhD[5]

Purpose: *The goal of this study was to compare the in vitro bioactivity in simulated body fluid (SBF) of commercially available dental implants.* ***Materials and Methods:*** *Bioactivity, according to ISO 23317, of commercially available dental implants with various surface modifications (BIO-surface, SLA, SLActive, TiUnite, and OsseoSpeed) was tested in SBF for 1 and 3 weeks. Surface characterizations, especially calcium and phosphorus surface content before and after the immersion in SBF, were performed. The effect of surface treatment on bioactivity was studied.* ***Results:*** *Differences between surfaces before immersion in SBF were confirmed by Raman spectroscopy, x-ray photoelectron spectroscopy (XPS), energy-dispersive x-ray spectroscopy (EDX), and scanning electron microscope (SEM) analysis. Calcium and phosphorus surface content was increasing within the tested period in the case of two (BIO-surface and SLActive) of the five tested dental implants. Calcium-phosphate precipitation was observed by SEM, XPS, EDX, and x-ray micro-diffraction (μ-XRD) analysis.* ***Conclusion:*** *Two (BIO-surface from LASAK and SLActive from Straumann) of the five tested dental implants were found to be bioactive, according to ISO 23317. Although it is difficult to unambiguously determine the properties that have influence on the hydroxyapatite precipitation rate, multiple properties that the two surfaces have in common were found.* Int J Oral Maxillofac Implants 2017;32:1221–1230. doi: 10.11607/jomi.5132

Keywords: *dental implant, in vitro bioactivity, ISO 23317, SBF, surface treatment*

The first materials with the ability to form a direct bond with living tissues were glasses discovered in 1969 by Hench.[1] These bioactive glasses based on the Na_2O-CaO-SiO_2 system were found to be able to induce calcium phosphate, namely, apatite, precipitation on their surface in the body environment. This apatite precipitation on the implanted material was described as being the key step in bone-material bond creation.[2]

Titanium has better mechanical properties than bioactive glasses and can be used for loaded implants. Brånemark et al were the first to describe direct contact of machined titanium with bone without an intermediate fibrous tissue layer.[3] The difference between bioactive glasses and the bond formation of machined titanium with bone is in the reaction rate; it takes days in the case of bioglass, while the machined titanium needs months to create a firm connection to the hard tissue.[4] In order to improve its osseointegration kinetics, the titanium surface must be modified—and it is a material that can be easily surface-modified in several ways—by blasting, electrochemical oxidation, acid etching, alkali etching, or by a combination of these methods.[5,6]

The simulated body fluid (SBF) test is a suitable, quick, inexpensive procedure for testing the bioactivity of implant materials. The SBF test was introduced by Kokubo and Takadama.[7] This procedure is able to reproduce in vivo bonelike apatite formation on bioactive materials as it simulates the aforementioned key step: the heterogeneous nucleation of apatite. The test can be reliably used to study the fastest implant-body interaction: the interaction with inorganic ions within the human body environment.

[1]Engineer, Research and Development Center for Dental Implantology and Tissue Regeneration, Českobrodská, Prague, Hloubětín, Czech Republic.
[2]Engineer, Research and Development Center for Dental Implantology and Tissue Regeneration, Českobrodská, Prague, Hloubětín, Czech Republic.
[3]CEO, Research and Development Center for Dental Implantology and Tissue Regeneration, Českobrodská, Prague, Hloubětín, Czech Republic.
[4]Researcher, Institute of Physics, Academy of Sciences of the Czech Republic, Cukrovarnická, Prague, Czech Republic.
[5]Researcher, Institute of Macromolecular Chemistry, Academy of Sciences of the Czech Republic, Heyrovského náměstí, Prague, Czech Republic.

Correspondence to: Mr Jan Šťovíček, Research and Development Center for Dental Implantology and Tissue Regeneration, Českobrodská 1047/46, 190 01 Prague 9 – Hloubětín, Czech Republic. Email: stovicek@lasak.cz

©2017 by Quintessence Publishing Co Inc.

© 2017 BY QUINTESSENCE PUBLISHING CO, INC. PRINTING OF THIS DOCUMENT IS RESTRICTED TO PERSONAL USE ONLY.
NO PART MAY BE REPRODUCED OR TRANSMITTED IN ANY FORM WITHOUT WRITTEN PERMISSION FROM THE PUBLISHER.

The SBF solution is an artificial model of the inorganic part of human plasma; it is a supersaturated solution with respect to calcium phosphates, ie, hydroxyapatite (HA), octacalcium phosphate (OCP), and dicalcium phosphate (DCPD). HA is the most thermodynamically stable in SBF, while DCPD can precipitate only when the concentration of Ca and P ions increases (eg, when it is released from substrate).[8]

Bohner and Lemaitre[9] reviewed possible mistakes in SBF preparation and suggested improvements in the testing, eg, using a reference material, filtration of the solution, and using the same material/liquid ratio for the tested samples. They pointed out that changes in the experimental setting (eg, volume/sample size ratio, dynamic vs static setting) could provoke a change in the outcome of the test. The quite-complicated preparation of the solution was criticized, and mixing in a 5% CO_2 atmosphere was recommended, as the carbonate content can be an issue.

The conventional SBF differs slightly from human plasma.[10,11] There is lower content of carbonate ions, as the calcium carbonate tends to precipitate from the solution.[12,13] Solutions with a higher amount of carbonates were tested, and this negatively influenced the SBF stability in terms of pH, ion concentrations, and cluster formation.[12,13] It is also necessary to buffer the in vitro solution; tris(hydroxymethyl)aminomethane and hydrochloric acid are recommended. It was also shown that a higher amount of chloride ions does not influence the SBF results.[12,13] Anyway, it is always important to compare data using one SBF composition, preferably the one prepared according to the ISO standard 23317.

The SBF test describes as bioactive any material that accelerates heterogeneous crystallization in this solution and does not take into account the complexity of the living body environment, the organic part of human body fluids, protein presence, or possible material cytotoxicity. Exceptions following from this simplification can occur: resorbable materials such as β-tricalcium phosphate or natural calcite showed false negative results in SBF,[7,9] while abalone shell showed a false positive test; this was attributed to the protein reactions.[7] This experience must be considered when testing new materials, and special attention should be given to resorbable materials or materials containing biologic components. Even the SBF test cannot describe the macrophage action, osteoblast stem cell attachments, or osteoblast proliferation.[11] The bioactivity in SBF does not guarantee successful implantation. The success of a dental implant is influenced by many factors,[14] including the patient condition, the doctor's experience, and the set of implant system qualities.

The SBF test, with its long history in bioactive materials research, is a useful test describing the primary and fastest actions during implant contact with plasma, ie, ion interaction. This interaction is crucial and can influence follow-up processes.[11] The Ca-P layer created in the SBF solution was, afterward, clinically identified on many bioactive materials, and even if a crystalline Ca-P layer may not be formed in vivo to such an extent as in vitro (for example, due to protein adsorption), the quick adsorption of calcium and phosphate ions on the surface of bioactive materials may play an important role in altering subsequent steps in the tissue–biomaterial interaction cascade.

The thin apatite layer formation was confirmed to be the first step in the bone–bioactive material bond formation in vivo.[15,16] Osteoblasts proliferate on this apatite, as it is very similar to the mineral phase in a bone. Subsequently, osteoblasts form a new bone, and a chemical bond between the mineral phase and the thin apatite layer is created to decrease the interfacial energy between them.[17]

Several studies confirmed this correlation between Ca-P layer formation in the in vitro SBF test and in vivo reality.[7,15,18] Even a valid ISO standard (ISO 23317) comprising the SBF test was published. The in vivo bioactivity was precisely reproduced by the apatite-forming ability in the SBF in the case of sintered HA, P_2O_5–Na_2O–CaO–SiO_2 glasses,[7] P_2O_5-free Na_2O–CaO–SiO_2 glasses,[15] or glass-ceramics.[18] Titanium and surface-treated titanium are also not an exception for SBF testing. The good correlation of in vivo and in vitro testing has already been shown in the case of titanium and modified titanium.[19–21] A significant difference in bone-to-implant contact (BIC) was observed for the alkali-treated titanium implant and machined titanium[4,21] during the early stages of healing (2 to 5 weeks). The chemically treated titanium showed more rapid BIC formation. This corresponds to in vitro tests in SBF.[22–24]

Based on the aforementioned information, it is suggested that the SBF test is a reliable method for titanium dental implant bioactivity comparison. The material does not belong to the known SBF test exceptions. This study does not deal with a new material in this case, but tests one single property of already successfully applied commercial products.

None of the chosen products contain proteins, toxic compounds, or resorbable calcium phosphate on their surface, and no other fact known to devalue the SBF test results was found, so the SBF test was accepted to be a relevant method for predicting the in vivo bone-bonding ability of the titanium dental implants.

Complicated titanium dental implant surfaces have been developed in recent years to provide a product with excellent clinical performance. A surface with bone-bonding ability is necessary. Thus, various original surface modifications have been introduced to the market, and their extraordinary osseointegration

© 2017 BY QUINTESSENCE PUBLISHING CO, INC. PRINTING OF THIS DOCUMENT IS RESTRICTED TO PERSONAL USE ONLY.
NO PART MAY BE REPRODUCED OR TRANSMITTED IN ANY FORM WITHOUT WRITTEN PERMISSION FROM THE PUBLISHER.

has been presented. Several studies dealing with detailed implant surface descriptions have been published.[5,7,25–29] Many factors such as oxide thickness, micropore configurations, chemical composition, and crystal structures influence the implant-bone behavior, and they can work synergistically.[30] A minor difference in the production technology, such as the method of packing, could affect the product property.[31] That is why not only individual treatments, but real systems should be studied.

The aim of this study was to evaluate the calcium phosphate nucleation ability of five commercially available dental implants. The representatives of the currently used surfaces—blasted and acid-etched surface (SLA [Institut Straumann]); blasted and acid-etched surface, stored in NaCl solution (SLActive [Institut Straumann]); electrochemically oxidized (TiUnite [Nobel Biocare]); grit-blasted with chemical (fluoride) modification (OsseoSpeed [Astra Tech]); and the surface prepared by the combination of blasting, acid etching, and alkali etching (BIO-surface [LASAK])—were chosen.

MATERIALS AND METHODS

The simulated body fluid (SBF) test was performed with an ion concentration corresponding to ISO 23317. The solution was filtered. Calcium and phosphorus concentrations were checked in a certified laboratory. The solution was successfully tested with negative (titanium, machined) and positive (standard glass B according to ISO 23317) references for 1 week.

Implants with similar dimensions were immersed in SBF (37°C ± 0.2°C) for 1 and 3 weeks; 100 mL of SBF was used for each implant. The test was performed in plastic containers. One piece of implant for each treatment group and time was used.

BIO-surface Straight 3.7 × 14 mm, SLA 4.1 ×14 mm, SLActive 4.1 × 14 mm, TiUnite 3.75 × 13 mm, and OsseoSpeed 4 × 13 mm implants in original packaging were purchased. The SBF tests were done without any further modifications; the implants were used immediately after unpacking, and no rinsing was applied (the SLActive implant was wet at the beginning of the test). Abbreviations used in the article are summarized in Table 1.

The implant surfaces were characterized by the following methods.

The roughness of the surfaces before the immersion in SBF was evaluated with an optical profilometer, Alicona Infinite Focus. The measurements were performed at three different surface regions for each sample: flank, valley, and top. The Sa parameter (the arithmetic mean of the departures of the roughness area from the mean plane) was evaluated using a Gaussian 50 × 50-µm filter. The SA-0w sample was dried before the measurement.

Table 1 Abbreviations for Tested Implants

	Before immersion in SBF	After 1 wk in SBF	After 3 wk in SBF
BIO-surface (LASAK)	L-0w	L-1w	L-3w
SLA (Institut Straumann)	S-0w	S-1w	S-3w
SLActive (Institut Straumann)	SA-0w	SA-1w	SA-3w
TiUnite (Nobel Biocare)	N-0w	N-1w	N-3w
OsseoSpeed (Astra Tech)	A-0w	A-1w	A-3w

Raman spectra were measured using a Raman microscope, Renishaw inVia. Measurements were performed in backscattering mode with a HeNe laser (633 nm) and objective 50×. Raman spectroscopy was used only for the original surface characterization.

The x-ray photoelectron spectroscopy (XPS) photoelectron spectra for quantitative surface analysis were recorded by an angle-resolved photoelectron spectrometer, ADES 400 (VG Scientific), operating at a base pressure of 1×10^{-10} Torr. The system is equipped with an x-ray excitation source and a rotatable hemispherical electron energy analyzer. Photoelectron spectra were recorded using Mg Kα radiation (1,253.6 eV), an angle of incidence of 70 degrees, an angle of emission of 0 degrees with respect to the surface normal, and pass energy of 100 eV. Atomic concentrations of elements found at the near-surface regions of samples were determined from photoelectron peak areas after Shirley's inelastic background subtraction, corrected for photoionization cross sections,[32] inelastic mean free paths of photoelectrons,[33] and the transmission function of the spectrometer used.[34] Samples (before and after immersion in SBF) were inserted in the ultrahigh vacuum chamber of the spectrometer without any surface cleaning, directly after unpacking. Only the SA-0w sample was rinsed with distilled water in order to remove salt from the storage solution. No surface cleaning was performed in the spectrometer.

Other XPS spectra were used for a structure analysis of the 0w samples. These spectra were recorded with the AXIS-Supra photoelectron spectrometer (Kratos Analytical), using monochromatized Al Kα radiation (1,486.6 eV, 300 W, analyzed area 0.7 × 0.3 mm^2). Before introduction into the spectrometer chamber, the samples did not undergo any surface cleaning treatment. The Kratos magnetic confinement charge compensation system was used during the analysis. The shift in energy due to the surface charging effect, even after it had been compensated, was calibrated to

© 2017 BY QUINTESSENCE PUBLISHING CO, INC. PRINTING OF THIS DOCUMENT IS RESTRICTED TO PERSONAL USE ONLY.
NO PART MAY BE REPRODUCED OR TRANSMITTED IN ANY FORM WITHOUT WRITTEN PERMISSION FROM THE PUBLISHER.

a binding energy of C 1s (285.0 eV). The high-energy resolved spectra of Ti 2p, P 2p, Na 1s, O 1s, and C 1s were collected in constant analyzer energy mode with pass energy of 10 eV and a step of 0.05 eV, resulting in an overall energy resolution of 0.45 eV, measured on the Ag $3d_{5/2}$ line width (FWHM). Selected spectra were analyzed by peak fit using Gaussian–Lorentzian sum functions.

Implants before and after the SBF test were placed in a scanning electron microscope (SEM) Vega II LSU (Tescan), and the images of their surfaces were taken with magnifications of 1,000× and 10,000×. A 10-kV accelerating voltage was used for observing the original surface morphology and changes after immersion in the SBF, including the growth of calcium phosphate crystals. Energy-dispersive x-ray spectroscopy (EDX), with original software Quantax (Bruker), was employed to identify the elements present on the implant surfaces. The spectra were taken for 100 seconds under the following conditions: 10 kV, working distance between the detector and the beam focal point (WD & Z) of 15.5 mm, magnification 500×. One region was analyzed per 0w and 1w implants, and three regions were analyzed per 3w implants. The means and standard deviations were calculated for the 3w samples. Similar standard deviations would be expected for the 0w and 1w samples.

The crystals grown on the surface of the 3w samples were identified by means of x-ray micro-diffraction (μ-XRD). The micro-diffraction experiments were performed as described elsewhere[35,36] using a PANalytical X'PertPRO diffractometer. A CoKα tube with point focus, an x-ray mono-capillary with a diameter of 0.1 mm in the primary beam path, and a multichannel detector X'Celerator with an anti-scatter shield in the diffracted beam path were used. A sample holder was adapted by adding vertical axis adjustment (a Huber 1005 goniometric head). It was assumed that the surface layer produced was very thin, so it was decided to fix the angle of the incident beam to 1.5 degrees to suppress the penetration depth and to enhance the signal of the layer.

The x-ray patterns were measured in the range of 3 to 70 degrees 2θ with a step of 0.0334 degrees and 2,500 seconds counting per step. A 2.5-mm anti-scatter slit and Fe beta filter were used in the diffracted beam. The duration of the scan was approximately 11.5 hours. The μ-XRD patterns were not pretreated before interpretation, as no background correction was needed. Qualitative analysis was performed with the HighScorePlus software package (PANalytical, version 4.6.1) and JCPDS PDF-4 database.[37]

No analysis was done on the SLActive packaging solution in the present study. However, previous studies[29] claim that 0.9% NaCl is used as the storage solution.

RESULTS

Surface Roughness

The evaluation of the surface roughness is depicted in Fig 1. The surface roughness did not vary dramatically between flank, valley, and top on any sample (the maximum relative standard deviation between flank, valley, and top was 12%). The sample L-0w showed the highest values of Sa parameter, followed by the samples SA-0w and S-0w.

Raman Analysis

Differences between surfaces were found with the Raman spectroscopy and can be seen in Fig 2.

The N-0w sample shows anatase Raman bands. Typical Raman bands for rutile were found in the A-0w.[38] A very weak spectrum was obtained by measuring the S-0w and SA-0w samples, which can be caused by the amorphous character of the titanium oxide. After multiplying the data, rutile bands can be observed in some cases. Individual bands of the spectrum L-0w are described in Fig 3.[38–40] These bands correspond to sodium titanate,[41] synthesized and described by Kokubo et al repetitively[24,42] as $Na_xH_{2-x}Ti_3O_7$; $0 < x < 2$.

XPS Analysis

The results of the elemental XPS analysis of the implants before and after immersion in SBF can be seen in Table 2. Carbon contamination was detected on all surfaces. Its initial value recorded from the as-received sample surfaces ranged from 20 to 36 at.% and rose after immersion in the SBF. Only TiUnite revealed a drop in carbon content following the immersion, likely due to the highest starting value of the carbon content and a deposited overlayer that covered the N-3w surface. The oxygen concentration behaved similarly to the carbon. As expected, titanium concentration dropped after the immersion for all samples, most strongly for the BIO-surface, indicating possible growth of HA. Ca and P concentration originating from the SBF rose significantly in time for the BIO-surface and SLActive surface (Fig 4). However, the Ca/P ratio approached closer to HA (1.67) only for the BIO-surface (1.33). The ratio reached ≤ 1 values for other samples.

In conclusion, all the samples exhibited a certain content of Ca and P on the surface after 1 or 3 weeks in the SBF. However, this content was approximately 1% to 2% on most samples, which rather corresponds to adsorption only. The only surfaces with higher content, indicating the HA overlayer, were the BIO-surface and SLActive surface. The thickest and most homogeneous HA overlayer was found for the L-3w sample with very weak Ti 2p spectral intensity from the substrate.

Besides the elemental quantitative surface analysis, a chemical bonding analysis was performed

© 2017 BY QUINTESSENCE PUBLISHING CO, INC. PRINTING OF THIS DOCUMENT IS RESTRICTED TO PERSONAL USE ONLY.
NO PART MAY BE REPRODUCED OR TRANSMITTED IN ANY FORM WITHOUT WRITTEN PERMISSION FROM THE PUBLISHER.

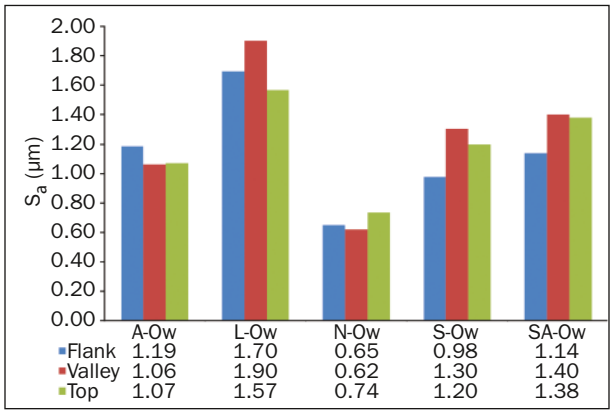

Fig 1 Roughness of the different surface regions of the samples.

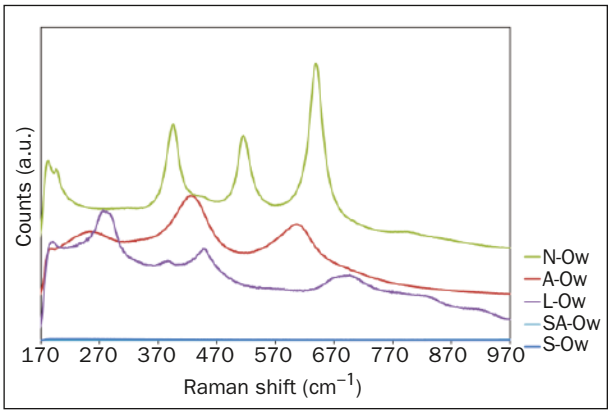

Fig 2 Raman spectra of all examined implants.

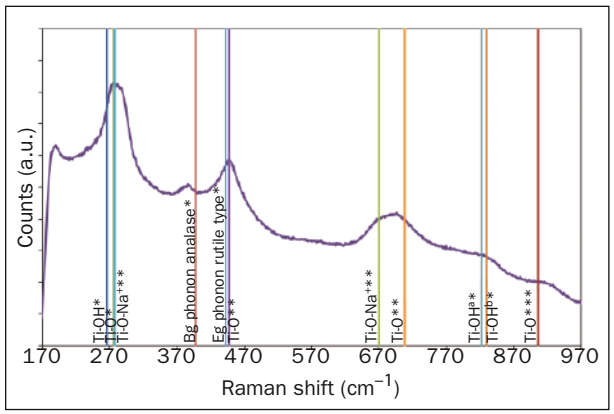

Fig 3 Raman spectra of implant L-0w. References *38, **39, ***40 are marked.

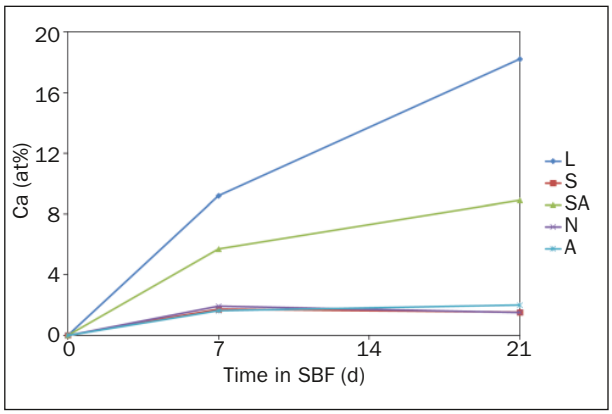

Fig 4 Content of Ca (in atomic %) on the implant surface after 0, 1, and 3 weeks in SBF (determined by means of XPS).

for the nonimmersed samples. For this purpose, higher-resolution spectra were recorded with an AXIS-Supra spectrometer. The spectra that shifted in energy by surface charging were corrected with respect to the C 1s peak maximum at 285.0 eV. The photoelectron spectra of C 1s, Ti 2p, O 1s, Na 1s, and P 2p transitions, recorded from the analyzed sample surfaces before the immersion in the SBF, are displayed in Figs 5 to 9. Electron inelastic background was removed from the spectra, and the spectra were normalized in intensity to unity.

The C 1s spectra, shown in Fig 5, were peak-fitted into five different bonding states, as illustrated in the bottom spectrum. Individual lines are ascribed to the following bonding states: The spectral lines at 282.2 and 283.8 eV were ascribed to C-Ti[43]; the spectral line at 285 eV was ascribed to C-C and C-H; that at 286.5 eV was ascribed to C-O; and that at 288.6 eV was ascribed to C = O.[44] The Ti 2p spectra, shown in Fig 6, exhibit peaks from Ti $2p_{3/2}$ and Ti $2p_{1/2}$ transitions located at 458.8 and 464 eV, respectively. They represent Ti in TiO_2[44] with a weak signal from Ti in substoichiometric TiO_x. The Ti $2p_{3/2}$ intensity

Table 2 XPS Analysis Before and After Immersion in SBF (in atomic %)

	C	O	Ti	Na	P	Cl	F	Ca
L-0w	29.5	49.2	16.2	5.1	0.0	0.0	0.0	0.0
L-1w	43.7	21.4	16.1	1.8	7.7	0.0	0.0	9.2
L-3w	54.2	10.0	1.1	2.7	13.7	0.0	0.0	18.2
S-0w	26.4	55.5	18.0	0.0	0.0	0.0	0.0	0.0
S-1w	32.1	47.6	12.2	1.9	2.3	1.0	1.0	1.7
S-3w	38.2	45.5	11.5	1.1	1.9	0.3	0.0	1.5
SA-0w	19.9	59.9	20.2	0.0	0.0	0.0	0.0	0.0
SA-1w	52.5	23.5	14.5	1.5	2.2	0.0	0.0	5.7
SA-3w	55.9	19.2	7.1	0.8	8.0	0.0	0.0	8.9
N-0w	36.0	48.1	11.9	0.0	1.4	0.6	2.0	0.0
N-1w	32.0	48.9	9.0	2.0	5.9	0.3	0.0	1.9
N-3w	29.4	54.2	7.3	1.6	5.8	0.0	0.0	1.5
A-0w	29.8	53.4	16.8	0.0	0.0	0.0	0.0	0.0
A-1w	44.1	40.9	10.1	1.2	1.2	0.8	0.0	1.6
A-3w	38.5	44.5	12.2	0.0	2.8	0.0	0.0	2.0

Estimated relative standard deviation is up to 10%.

© 2017 BY QUINTESSENCE PUBLISHING CO, INC. PRINTING OF THIS DOCUMENT IS RESTRICTED TO PERSONAL USE ONLY.
NO PART MAY BE REPRODUCED OR TRANSMITTED IN ANY FORM WITHOUT WRITTEN PERMISSION FROM THE PUBLISHER.

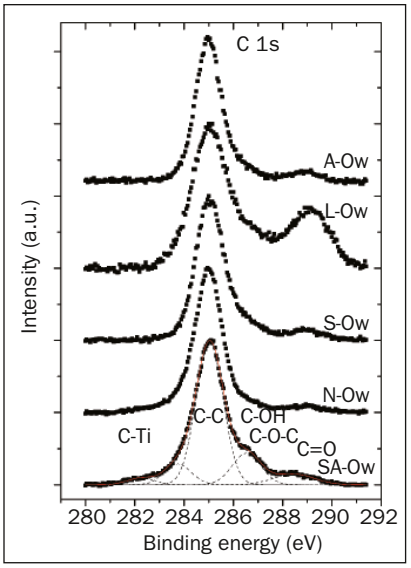

Fig 5 C 1s photoelectron spectra of sample surfaces before immersion in SBF.

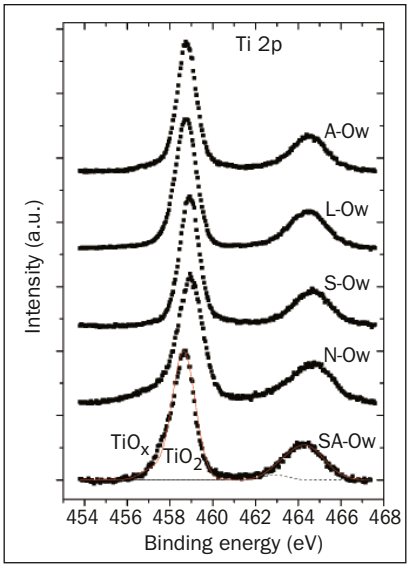

Fig 6 Ti 2p photoelectron spectra of sample surfaces before immersion in SBF.

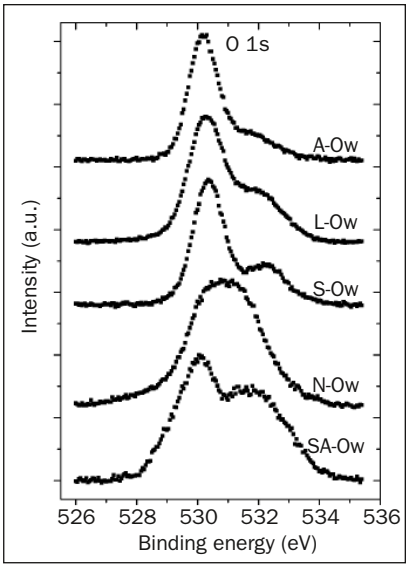

Fig 7 O 1s photoelectron spectra of sample surfaces before immersion in SBF.

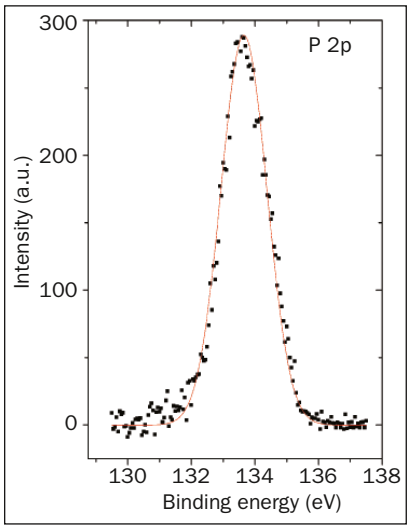

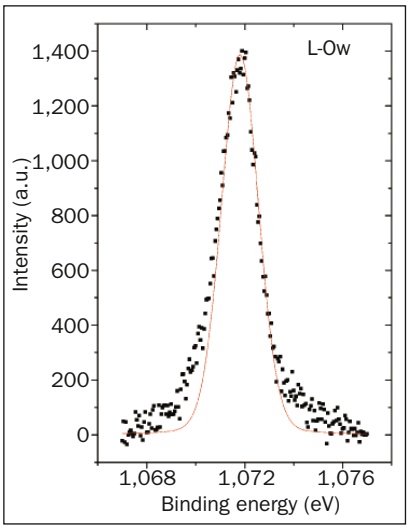

Fig 8 *(Left)* P 2p photoelectron spectrum of N-0w sample surface before immersion in SBF.

Fig 9 *(Right)* Na 1s photoelectron spectrum of L-0w sample surface before immersion in SBF.

from Ti in sodium titanates, $Na_2Ti_3O_7$ and Na_2TiO_3, located close to that for TiO_2 (458.2 and 458.3 eV[45]), can be hidden in the dominating spectral signal from Ti in TiO_2. The O 1s spectra shown in Fig 7 exhibit a two-peak structure. The intensity at 530 eV originates from O bonded to Ti. A rather wide peak located at approximately 532.5 eV comprises several bonding states of oxygen: O in –OH, O bonded to carbon, and O in titanates. Furthermore, the O-P line (531.3 eV) probably coincides with the other lines in sample N-0w.[44,46,47] Due to their complexity, the O 1s spectra were not fitted. The P 2p spectrum of the N-0w sample is shown in Fig 8 and can be ascribed to the phosphate bonding state. The Na 1s spectrum recorded from the L-0w sample surface, shown in Fig 9, was fitted by using one line mapping the dominating spectral signal peaked at 1,071.8 eV. This can be ascribed to Na in $Na_2Ti_3O_7$,[48] in agreement with the Raman spectra. Note that the region of Na 1s spectrum is overlapped with a weaker and wide spectral signal from Ti LMM Auger transition. As a consequence, some excess spectral signal is clearly visible on both sides of the fitting sub-line.

EDX Analysis

C, N, O, Ti, P, Ca, Na, F, K, Mg, and Cl were found on the implants. The presence of elements with low molecular weight (C, N, and O) was measured; however, these elements were not included in the quantitative comparison because of the extreme error (the EDX quantification of light elements is generally difficult), and the rest of the element amounts were normalized to 100%. The results can be seen in Table 3. Standard deviations were calculated for the 3w samples; similar deviations can be expected for the other samples. The largest deviations are observed on Ti, Ca, and P

© 2017 BY QUINTESSENCE PUBLISHING CO, INC. PRINTING OF THIS DOCUMENT IS RESTRICTED TO PERSONAL USE ONLY.
NO PART MAY BE REPRODUCED OR TRANSMITTED IN ANY FORM WITHOUT WRITTEN PERMISSION FROM THE PUBLISHER.

Table 3 EDX Analysis Before and After Immersion in SBF (in atomic %)

	Ti	Na	P	Cl	F	K	Mg	Ca
L-0w	86	14	0	0	0	0	0	0
L-1w	77	9	3	0	0	0	3	8
L-3w	40 (2)	4 (1)	19 (2)	1 (1)	1 (2)	0 (1)	2 (1)	33 (3)
S-0w	100	0	0	0	0	0	0	0
S-1w	100	0	0	0	0	0	0	0
S-3w	100 (0)	0 (0)	0 (0)	0 (0)	0 (0)	0 (0)	0 (0)	0 (0)
SA-0w	84	10	0	6	0	0	0	0
SA-1w	100	0	0	0	0	0	0	0
SA-3w	86 (16)	0 (0)	6 (7)	0 (0)	0 (0)	0 (0)	0 (1)	8 (8)
N-0w	81	0	19	0	0	0	0	0
N-1w	83	0	20	0	0	0	0	0
N-3w	81 (3)	1 (2)	18 (5)	0 (0)	0 (0)	0 (0)	0 (0)	0 (0)
A-0w	100	0	0	0	0	0	0	0
A-1w	99	1	0	0	0	0	0	0
A-3w	100 (0)	0 (0)	0 (0)	0 (0)	0 (0)	0 (0)	0 (0)	0 (0)

Standard deviations of the element amounts in 3w samples are given in parentheses. The other values are expected to have standard deviations at a similar level.

amounts in the SA-3w samples; this is probably caused by the nonhomogeneous distribution of growing HA crystals. Also, the high relative deviations of the less abundant elements might be caused by nonhomogeneous distribution.

Ca and P were detected on L-1w (2.7), L-3w (1.7), and SA-3w (1.2), with the Ca/P ratio given in brackets. The significant change in the Ca presence on the surface can be seen in Fig 10.

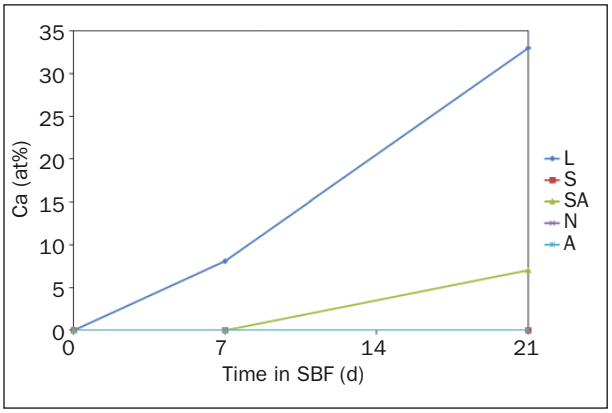

Fig 10 Content of Ca (in atomic %) on the implant surface after 0, 1, and 3 weeks in SBF (determined by means of EDX).

SEM Analysis

The differences and similarities of the implant surface structures at magnifications 10,000× were studied. Each implant has its own unique appearance with visible microroughness; only the S-0w and SA-0w are not distinguishable by the SEM images. Sharp pits from acid etching could be seen on SA-0w and S-0w. A macrorough surface with etch pits covered by a structure resembling 0.5- to 2-µm stars was observed on the L-0w. Grit-blast pits with fine-irregular valley covered facets were present on the A-0w implant. Pores with a diameter in the range of approximately 0.5 to 3 µm with elevated margins were observed on the N-0w.

No calcium phosphate crystals were found on the surfaces of the tested implants after 1 week in the SBF. No significant changes, compared with the initial SEM images, were observed. Typical calcium phosphate spheres were found only on the L-3w and SA-3w samples. No significant changes, compared with the initial SEM images, were observed in the A-3w, N-3w, and S-3w samples. The SEM micrographs can be seen in Figs 11 to 20.

µ-XRD Analysis

Since the calcium phosphate spheres were found only on the SEM images of the L-3w and SA-3w samples, the µ-XRD analysis was performed only for these two samples. The subsequent x-ray patterns (Fig 21) confirmed the presence of HA. Also, the diffraction maxima of titanium were identified. The TiO_2 lines were not observed at all, implying its amorphous character. Only extremely weak lines of sodium titanate were identified; moreover, these lines partially overlay with another diffraction maxima. This sodium titanate is poorly crystalized, as it is produced by the alkali etching of the Ti surface. Additionally, the thin layer of sodium titanate is covered by HA, which attenuates the signal from the inferior layer and bulk material of the core of the implant. Similarly, it is clearly visible in

© 2017 BY QUINTESSENCE PUBLISHING CO, INC. PRINTING OF THIS DOCUMENT IS RESTRICTED TO PERSONAL USE ONLY.
NO PART MAY BE REPRODUCED OR TRANSMITTED IN ANY FORM WITHOUT WRITTEN PERMISSION FROM THE PUBLISHER.

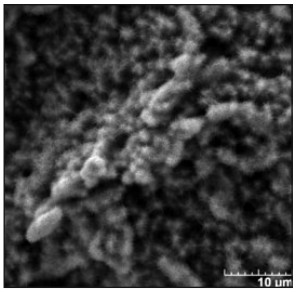

Fig 11 SEM micrograph of L-0w.

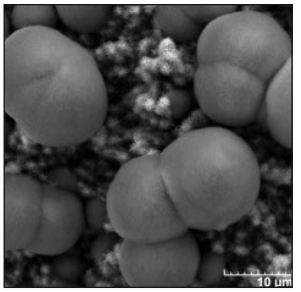

Fig 12 SEM micrograph of L-3w.

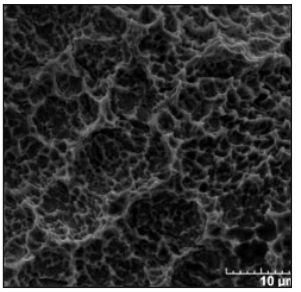

Fig 13 SEM micrograph of S-0w.

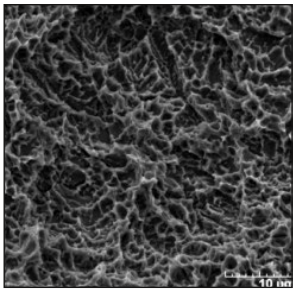

Fig 14 SEM micrograph of S-3w.

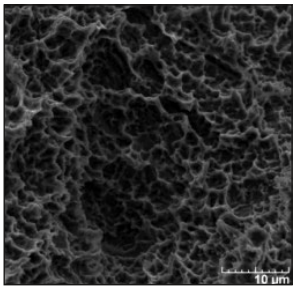

Fig 15 SEM micrograph of SA-0w.

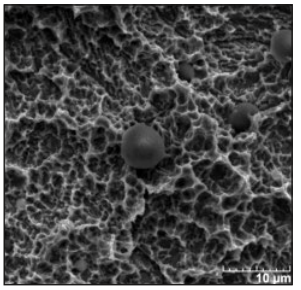

Fig 16 SEM micrograph of SA-3w.

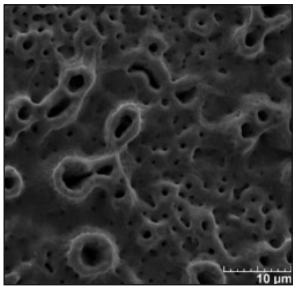

Fig 17 SEM micrograph of N-0w.

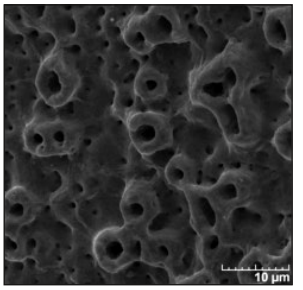

Fig 18 SEM micrograph of N-3w.

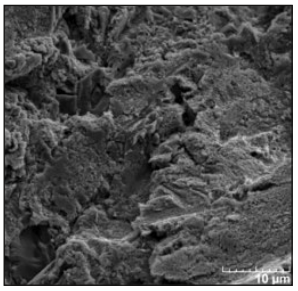

Fig 19 SEM micrograph of A-0w.

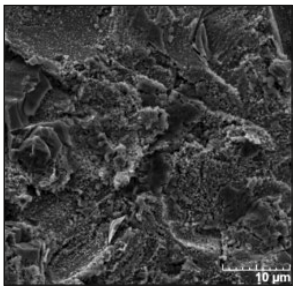

Fig 20 SEM micrograph of A-3w.

the intensities of the titanium diffraction lines. Their intensity is also lower than the one expected for a pristine implant. The difference in intensities between samples L-3w and SA-3w (Fig 21) implies a larger amount of HA on the sample L-3w compared with the sample SA-3w.

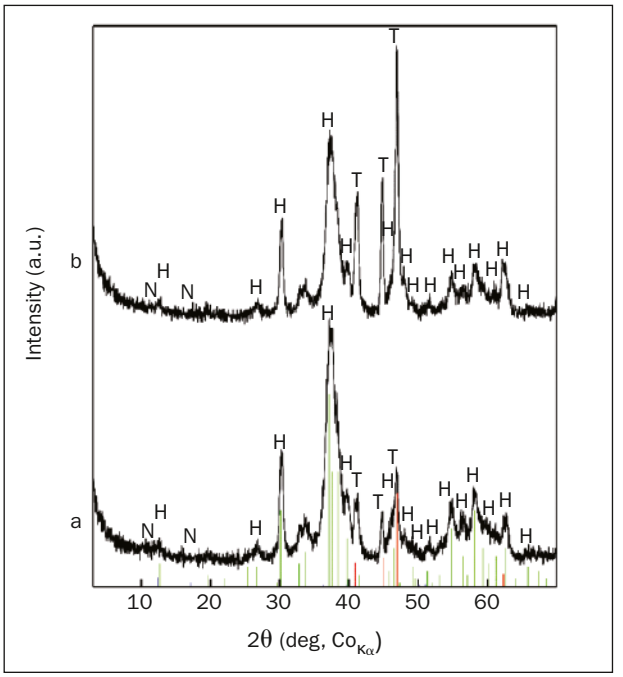

Fig 21 XRD patterns of the *(a)* L-3w and *(b)* SA-3w samples. The diffraction maxima of hydroxyapatite (H), titanium (T), and sodium titanate (N) are present.

DISCUSSION

The SBF test of the commercial implants performed in this study showed significant differences between particular implants. Only two of the five tested implants (BIO-surface and SLActive) seem to have surface-enhancing calcium phosphate precipitation. The calcium phosphate precipitate growing on the real implants in this study was confirmed by the means of SEM, EDX, XPS, and μ-XRD measurements.

To explain the reasons for the differences in in vitro bioactivity, a complex description of the implants should be undertaken. The surface characterization methods in this work were chosen to reveal the structure, chemical composition, and crystal structure.

The surface roughness has an effect especially on the protein and cell response. However, its influence

© 2017 BY QUINTESSENCE PUBLISHING CO, INC. PRINTING OF THIS DOCUMENT IS RESTRICTED TO PERSONAL USE ONLY.
NO PART MAY BE REPRODUCED OR TRANSMITTED IN ANY FORM WITHOUT WRITTEN PERMISSION FROM THE PUBLISHER.

on the SBF response was also described.[49] In the present study, the only two samples with positive SBF response were the two with the two highest Sa values. The comparison of the roughness values with the aforementioned study is difficult, since different measurement and evaluation methods were used.

All the implants have microstructured surfaces. The BIO-surface implant has the finest observed structure, with a surface area 2 orders of magnitude higher than pure titanium,[50] which means a higher area for the SBF (or blood plasma) reaction with the implant surface. The SLActive surface seems to be very similar to SLA in the SEM micrographs. The distinct bioactivity of SLA and SLActive, according to the SBF test, implies, most likely, the importance of the combination of an appropriate morphology with other properties.

The chemical composition is similar for all the implants before immersion in the SBF. The EDX and XPS analyses revealed a major content of Ti and O in all samples. Moreover, Na is present on the surface of the SA-0w (accompanied by chlorine) and L-0w samples, and P was detected on the surface of the N-0w sample. The Na and Cl on the noncleaned SLActive surface were identified as the storage solution residues, as they disappear after rinsing with water. All the implants were contaminated by carbohydrates; the amounts of carbon are comparable with other studies.[29] The C contamination can be caused by atmospheric pollution or by technology (eg, washing). The differences between the XPS and EDX results were caused by distinct information depth.

The chemical bonding analysis by means of high-resolution XPS revealed the presence of dominating titanium dioxide and minor substoichiometric titanium oxides on the surface of all samples. However, the bands of titanium oxides may interfere with the bands of titanates, which were identified on the BIO-surface with Raman spectroscopy.

The calcium and phosphorus ion adsorption and apatite crystal growth on alkali-treated titanium, as well as the lack of Ca and P adsorption on only acid-treated titanium in the SBF, were described before.[51] No references for SLActive in SBF were found.

The calcium phosphate spheres, identified as HA by means of μ-XRD, were observed only on the BIO-surface and SLActive surface. There are a couple of properties that these surfaces have in common. Both surfaces are the roughest ones among the tested surfaces. However, the differences of surface roughness are not as significant in some cases (eg, SLA vs SLActive), so perhaps the roughness itself is not a key to bioactivity; nevertheless, it can play an important part in combination with other surface properties. Wettability was not measured in this work, but based on references, the BIO-surface and SLActive surface are hydrophilic with high surface free energy.[52,53] Sodium compounds (sodium chloride and sodium titanate) are present on these surfaces. Sodium chloride was detected on the SLActive surface as the storage solution residue. Sodium titanate was detected only on the BIO-surface in this study; however, the detectable titanate on the SLActive surface was published previously.[29] The evidence of sodium titanate on the SLActive surface can be supported by the fact that the Na/Cl ratio determined on the SA-0w surface with EDX is > 1, so that part of the Na atoms is bound to other than chlorine particles. These Na atoms can co-form an alkali titanate layer.

Kim et al[22] described a mechanism of ionic exchange leading to HA crystallization from SBF. In this mechanism, the alkali titanate layer plays the key role. This, together with the high surface roughness and high wettability, can contribute to the HA formation on the surfaces of the two samples.

However, the HA deposition rate can also be affected by other factors, eg, carbon contamination. Nonpolar carbon contaminants can negatively influence the wettability of the surface. Nevertheless, the complete effect of the carbon contaminants on the HA deposition rate remains unclear.

CONCLUSIONS

According to the in vitro SBF experiment, both the BIO-surface (LASAK) and SLActive (Institut Straumann) implants accelerate calcium phosphate forming on their surfaces compared with the other commercial implants tested in this study: SLA (Institut Straumann), TiUnite (Nobel Biocare), and OsseoSpeed (Astra Tech).

The implant surface is a complex system with several properties that can affect the calcium phosphate deposition rate. Therefore, it is very difficult to identify a single property that has an impact on faster HA crystallization from SBF. However, it can be concluded that the only two samples the HA layer was observed on have multiple properties in common: high surface roughness, high wettability, and a certain content of the alkali titanate hydrogel.

ACKNOWLEDGMENTS

The authors reported no conflicts of interest related to this study.

REFERENCES

1. Hench LL. The story of Bioglass. J Mater Sci Mater Med 2006;17:967–978.
2. Hench LL, Wilson J. An Introduction to Bioceramics. Singapore: World Scientific, 1999.
3. Brånemark PI, Adell R, Breine U, Hansson BO, Lindström J, Ohlsson A. Intra-osseous anchorage of dental prostheses. I. Experimental studies. Scand J Plast Reconstr Surg 1969;3:81–100.

© 2017 BY QUINTESSENCE PUBLISHING CO, INC. PRINTING OF THIS DOCUMENT IS RESTRICTED TO PERSONAL USE ONLY.
NO PART MAY BE REPRODUCED OR TRANSMITTED IN ANY FORM WITHOUT WRITTEN PERMISSION FROM THE PUBLISHER.

4. Strnad J, Strnad Z, Šesták J, Urban K, Povýšil C. Bio-activated titanium surface utilizable for mimetic bone implantation in dentistry—Part III: Surface characteristics and bone-implant contact formation. J Phys Chem Solids 2007;68:841–845.
5. Kanga BS, Sul YT, Oh SJ, Lee HJ, Albrektsson T. XPS, AES and SEM analysis of recent dental implants. Acta Biomater 2009;5:2222–2229.
6. Šimůnek A, Strnad J, Štěpánek A. Bioactive titanium implants for shorter healing period. Clin Oral Implants Res 2002;13(4).
7. Kokubo T, Takadama H. How useful is SBF in predicting in vivo bone bioactivity? Biomaterials 2006;27:2907–2915.
8. Lu X, Leng Y. Theoretical analysis of calcium phosphate precipitation in simulated body fluid. Biomaterials 2005;26:1097–1108.
9. Bohner M, Lemaitre J. Can bioactivity be tested in vitro with SBF solution? Biomaterials 2009;30:2175–2179.
10. Helebrant A, Jonášová L, Šanda L. The influence of simulated body fluid composition on carbonated hydroxyapatite formation. J Ceramics-Silikáty 2002;46:9–14.
11. Hench L. Chronology of bioactive glass development and clinical applications. NJGC 2013;3:67–73.
12. Oyane A, Kim HM, Furuya T, Kokubo T, Miyazaki T, Nakamura T. Preparation and assessment of revised simulated body fluids. J Biomed Mater Res A 2003;65:188–195.
13. Oyane A, Onuma K, Ito A, Kim HM, Kokubo T, Nakamura T. Formation and growth of clusters in conventional and new kinds of simulated body fluids. J Biomed Mater Res A 2003;64:339–348.
14. Porter JA, von Fraunhofer JA. Success or failure of dental implants? A literature review with treatment considerations. Gen Dent 2005;53:423–432.
15. Fujibayashi S, Neo M, Kim HM, Kokubo T, Nakamura T. A comparative study between in vivo bone ingrowth and in vitro apatite formation on Na2O-CaO-SiO2 glasses. Biomaterials 2003;24:1349–1356.
16. Neo M, Nakamura T, Ohtsuki C, Kokubo T, Yamamuro T. Apatite formation on three kinds of bioactive material at an early stage in vivo: A comparative study by transmission electron microscopy. J Biomed Mater Res 1993;27:999–1006.
17. Kokubo T, Kim HM, Kawashita M. Novel bioactive materials with different mechanical properties. Biomaterials 2003;24:2161–2175.
18. Kokubo T, Ito S, Huang ZT, et al. Ca,P-rich layer formed on high-strength bioactive glass-ceramic A-W. J Biomed Mater Res 1990;24:331–343.
19. Nishiguchi S, Fujibayashi S, Kim HM, Kokubo T, Nakamura T. Biology of alkali- and heat-treated titanium implants. J Biomed Mater Res A 2003;67:26–35.
20. Oron A, Agar G, Oron U, Stein A. Correlation between rate of bony ingrowth to stainless steel, pure titanium, and titanium alloy implants in vivo and formation of hydroxyapatite on their surfaces in vitro. J Biomed Mater Res A 2009;91:1006–1009.
21. Strnad J, Macháček J, Strnad Z, Povýšil C, Strnadová M. Alkali-modified titanium surface stimulating formation of bone-implant interface. Key Eng Mater 2008;361:749–752.
22. Kim HM, Miyaji F, Kokubo T, Nakamura T. Preparation of bioactive Ti and its alloys via simple chemical surface treatment. J Biomed Mater Res 1996;32:409–417.
23. Uchida M, Kim HM, Kokubo T, Fujibayashi S, Nakamura T. Effect of water treatment on the apatite-forming ability of NaOH-treated titanium metal. J Biomed Mater Res 2002;63:522–530.
24. Pattanayak DK, Kawai T, Matsushita T, Takadama H, Nakamura T, Kokubo T. Effect of HCl concentrations on apatite-forming ability of NaOH-HCl- and heat-treated titanium metal. J Mater Sci Mater Med 2009;20:2401–2411.
25. Castilho GA, Martins MD, Macedo WA. Surface characterization of titanium based dental implants. Braz J Phys 2006;36:1004–1008.
26. Sul YT, Byon E, Wennerberg A. Surface characteristics of electrochemically oxidized implants and acid-etched implants: Surface chemistry, morphology, pore configurations, oxide thickness, crystal structure, and roughness. Int J Oral Maxillofac Implants 2008;23:631–640.
27. Rodríguez-Rius D, García-Saban FJ. Physico-chemical characterization of the surface of 9 dental implants with 3 different surface treatments. Med Oral Patol Oral Cir Bucal 2005;10:58–65.
28. Sul YT, Jönsson J, Yoon GS, Johansson C. Resonance frequency measurements in vivo and related surface properties of magnesium-incorporated, micropatterned and magnesium-incorporated TiUnite, Osseotite, SLA and TiOblast implants. Clin Oral Implants Res 2009;20:1146–1155.
29. Zinelis S, Silikas N, Thomas A, Syres K, Eliades G. Surface characterization of SLActive dental implants. Eur J Esthet Dent 2012;7:72–92.
30. Sul YT, Johansson CB, Jeong Y, Wennerberg A, Albrektsson T. Resonance frequency and removal torque analysis of implants with turned and anodized surface oxides. Clin Oral Implants Res 2002;13:252–259.
31. Buser D, Broggini N, Wieland M, et al. Enhanced bone apposition to a chemically modified SLA titanium surface. J Dent Res 2004;83:529–533.
32. Band IM, Kharitonov YI, Trzhaskovskaya MB. Photoionization cross sections and photoelectron angular distributions for x-ray line energies in the range 0.132–4.509 keV targets: $1 \leq Z \leq 100$. At Data Nucl Data Tables 1979;23:443–505.
33. Tanuma S, Powell CJ, Penn DR. Calculations of electron inelastic mean free paths. IX. Data for 41 elemental solids over the 50 eV to 30 keV range. Surf Inter Anal 2011;43:689–713.
34. Jiříček P. Measurement of the transmission function of the hemispherical energy analyser of ADES 400 electron spectrometer. Czech J Phys 1994;44:261–267.
35. Švarcová S, Kočí E, Bezdička P, Hradil D, Hradilová J. Evaluation of laboratory powder x-ray micro-diffraction for applications in the field of cultural heritage and forensic science. Anal Bioanal Chem 2010;398:1061–1076.
36. Hradil D, Bezdička P, Hradilová J, Vašutová V. Microanalysis of clay-based pigments in paintings by XRD techniques. Microchem J 2016;125:10–20.
37. JCPDS PDF-4 Database. International Centre for Diffraction Data, Newtown Square, Pennsylvania, USA release 2016.
38. Qian L, Du Z, Yang S, Jin ZS. Raman study of titania nanotube by soft chemical process. J Molec Structure 2005;749:103–107.
39. Tian BL, Du ZL, Ma YM, et al. Raman investigation of sodium titanate nanotubes under hydrostatic pressures up to 26.9 GPa. Chin Phys Lett 2010;27:1–4.
40. Byeon SH, Lee SO, Kim H. Structure and Raman spectra of layered titanium oxides. J Solid State Chem 1997;130:110–116.
41. Sun X, Li Y. Synthesis and characterization of ion-exchangeable titanate nanotubes. Chemistry 2003;9:2229–2238.
42. Pattanayak DK, Matsushita T, Takadama H, et al. Fabrication of bioactive porous Ti metal with structure similar to human cancellous bone by selective laser melting. Bioceram Dev Appl 2011;1:1–3.
43. Bai WQ, Li LL, Wang XL, et al. Effects of Ti content on microstructure, mechanical and tribological properties of Ti-doped amorphous carbon multilayer films. Surf Coat Technol 2015;266:70–78.
44. Moulder JF, Stickle WF, Sobol PE, Bomben KD. In: Chastain J, Moulder JF (eds). Handbook of X-ray Photoelectron Spectroscopy: A Reference Book of Standard Spectra for Identification and Interpretation of XPS Data. Eden Prarie: Perkin-Elmer, 1992.
45. Song HY, Jiang HF, Liu T, Liu XQ, Meng GY. Preparation and photocatalytic activity of alkali titanate nano materials A2Ti(n)O(2n+1) (A = Li, Na and K). Mater Res Bull 2007;42:334–344.
46. Boyd AR, Meenan BJ, Leyland NS. Surface characterisation of the evolving nature of radio frequency (RF) magnetron sputter deposited calcium phosphate thin films after exposure to physiological solution. Surf Coat Technol 2006;200:6002–6013.
47. Takadama H, Kim HM, Kokubo T, Nakamura T. XPS study of the process of apatite formation on bioactive Ti-6Al-4V alloys in simulated body fluid. Sci Technol Adv Mater 2001;2:389–396.
48. Zhao M, Huang J, Guo X, et al. Preparation of $Na_2Ti_3O_7$/titanium peroxide composites and their adsorption property on cationic dyes. J Chemistry 2015;(2015):1–12.
49. Chen X, Nouri A, Li Y, Lin J, Hodgson PD, Wen C. Effect of surface roughness of Ti, Zr, and TiZr on apatite precipitation from simulated body fluid. Biotechnol Bioeng 2008;101:378–387.
50. Strnad J, Protivínský J, Strnad Z, Helebrant A. Early interaction of biomaterials with dynamic simulated body environment. In: Leng H, Chen CY (eds). Proceedings of 5th Asian Symposium on Biomedical Materials. Hong Kong: Hong Kong University of Science & Technology, 2001:51–55.
51. Strnad J, Protivínský J, Mazur D, et al. Interaction of acid and alkali treated titanium with dynamic simulated body environment. J Therm Anal Calorim 2004;76:17–31.
52. Strnad J, Urban K, Povysil C, Strnad Z. Secondary stability assessment of titanium implants with an alkali-etched surface: A resonance frequency analysis study in beagle dogs. Int J Oral Maxillofac Implants 2008;23:502–512.
53. Rupp F, Scheideler L, Olshanska N, de Wild M, Wieland M, Geis-Gerstorfer J. Enhancing surface free energy and hydrophilicity through chemical modification of microstructured titanium implant surfaces. J Biomed Mater Res A 2006;76:323–334.

© 2017 BY QUINTESSENCE PUBLISHING CO, INC. PRINTING OF THIS DOCUMENT IS RESTRICTED TO PERSONAL USE ONLY.
NO PART MAY BE REPRODUCED OR TRANSMITTED IN ANY FORM WITHOUT WRITTEN PERMISSION FROM THE PUBLISHER.